A Low Upper Threshold for Saltation-Mediated Triboluminescence at Gale Crater, Mars H. M. Sapers[1], J. L. Kloos[2], M. Baker[3], D. M. Fey[4], H. Kalucha[5], M. Lemmon[6], M. Minitti[7], C. Newman[8], J. E. Moores[1], [1]York University Centre for Research in Earth and Space Science (hsapers@yorku.ca), [2]University of Maryland, [3]Smithsonian Institution, [4]Malin Space Science Systems, San Diego, CA 92191-0148, USA [5]California Institute of Technology, Division of Geological and Planetary Sciences, [6]Space Science Institute, [7]Planetary Science Institute, [8]Aeolis research

Introduction: Laboratory studies suggest that saltation-driven grain-to-grain collisions are capable of producing triboelectric discharge in the hyperarid, near-surface atmosphere on Mars [1,2]. Saltation simulation experiments induced triboelectric discharge with a radiance of approximately 1.4 - 3.2 $\mu W/m^2/sr$ under a simulated Martian-atmospheric composition at 8 mbar pressure - capable of ionizing methane and providing a potential mechanism to explain the enigmatic seasonal variations of CH_4 and O_2 [3]. With observational evidence of wind-mediated saltation [4–7], saltation-induced triboelectric discharge is theorized to be common on Mars, but has yet to be observed *in situ*. We successfully carried out the fist *in situ* triboelectric observations carried out by the Mars Hands Lens Imager (MAHLI) onboard the Mars Science Laboratory (MSL) Curiosity Rover setting an upper threshold for triboelectric discharge that would not have a measurable effect on near-surface atmospheric composition.

The observed seasonal variation of CH_4 and O_2 in the Martian atmosphere is not fully explained by currently understood atmospheric or geological processes. The apparent correlation between CH_4 and O_2 variation suggests a potentially shared mechanism accounting for an increase in volume mixing ratios (VMR) during the northern spring/summer followed by apparent destruction during the northern summer and autumn (figure 1). An empirical study simulating saltating grains [3] indicated that saltation mediated triboelectric discharge is capable of ionizing argon, and therefore also CH_4 and O_2, providing a testable hypothesis for a mechanism behind CH_4 and O_2 depletion during dust storm season beginning ~Ls 180°–210° and ending ~Ls 330°–360° during the norther autumn and winter (figure 1). Methane is of particular interest as ~70% of methane of Earth is biogenic [8], as such, enigmatic sources and sinks of methane on Mars hinting at as of yet unknown processes remain a tantalizing biosignature potentially indicative of putative past or extant biological activity in the subsurface [9]. Subsurface methanogenic microorganisms on Earth produce methane through anaerobic chemoautolithic metabolisms, consistent with physicochemical conditions in the putatively habitable Martian subsurface [10].

Curiosity performed a 'Sands of Forvie' (a sand sheet is approximately 400 m x 1000 m in extent)

observing campaign between Sols 2989 and 3213 during the end of the windy season providing an opportunity to perform a night observation optimized to detect putative triboluminescence provided that it is occurring at the rate predicted by [3]. Further, we quantify an upper threshold if triboluminescence is not observed.
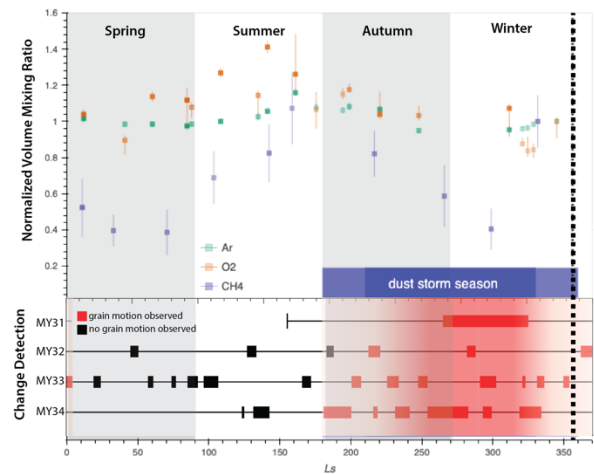
Figure 1: Normalized volume mixing ratios of Ar, O_2, and CH_4 in the near surface Martian atmosphere as measured by the Sample Analysis at Mars (SAM) instrument onboard Curiosity over Mars years 31-34 indicating the enigmatic seasonal cycle of CH_4 and O_2 with a decrease during the dust storm season. Data from [11,12] (top). MARDI change detection observations from Mars year 31-34 indicating observed grain movement (red) and no observed grain movement (black; bottom). The dotted line indicates the L_s of the triboelectric observation at the end of the windy season.

Observations: The Mars Science Laboratory (MSL) rover, Curiosity, performed a 'Sands of Forvie' observing campaign between Sols 2989 and 3213 during the end of the windy season providing an opportunity to perform a night observation optimized to detect triboluminescence. The Sands of Forvie sand sheet is approximately 400 m x 1000 m in extent. Due to a combination of spectral range, sensitivity, field of view, and operability, MAHLI [13] was selected for the

observation. Three main observational experiments were executed:

1) Triboluminescence observation, (Sol 3017): Seventeen 60-second full-frame MAHLI images were acquired at night (without Phobos in the sky) to capture a signal of saltation-mediated triboluminescence. As documented in a corresponding MAHLI image acquired during daylight hours, the scene included the sand sheet, foreground rocks, the local horizon, and the sky (figure 2);

2) Wind assessment (Sols 3022, 3024): A set of change detection images, view acquired with the fixed-pointing Mars Descent Imager (MARDI) camera, were used to assess wind/saltation conditions present around the time of the triboluminescence experiment;

3) Phobos-shine observation (Sol 3215); Seventeen 60-second exposures were acquired of the rover's remote sensing mast (RSM) with the white RSM angled to reflect Phobos-light. A corresponding daytime context image was also obtained (figure 3).

Image processing: Images were downlinked as losslessly compressed raster 8 bit files using first difference Huffman compression. Following decompression, the data were decompanded into 12 bits and stored as 16 bit integers. Radiometric calibration was achieved using the standard MAHLI spatial domain calibration pipeline [9] including dark current compensation, shutter smear migration, and flat field correction. The radiometrically calibrated and color corrected prepointed daylight images were used for masking.

Triboelectric observation: Four areas on the daylight pre-pointed image were identified and masked using RGB band ratios: sky, foreground, sand sheet, and the Greenheugh pediment (figure 3). The brightest and darkest $1/6^{th}$ pixels were masked in each of the 17 images in the night sequence, all 17 images were then stacked and averaged. The mean digital number (DN) value was then calculated for each of the masked areas identified in the pre-pointed image.

Figure 3: Pre-pointed daylight image (L) and average triboluminescence image (R) indicated no increased signal in the sand sheet attributable to triboluminescence.

Phobos-Shine: An offset between the pre-pointed daylight image and the 17 frame night sequence attrib-

uted to tolerance in repositing the rover arm precluded direct masking based on the daylight image. The brightest and darkest $1/6^{th}$ pixels were masked in each of the 17 images in the night sequence, all 17 images were then stacked and averaged. Using the signal in the processed Phobos-shine image, the area of Phobos-light reflected in the RSM was masked and the average DN value for the green channel was calculated after applying a median filter.
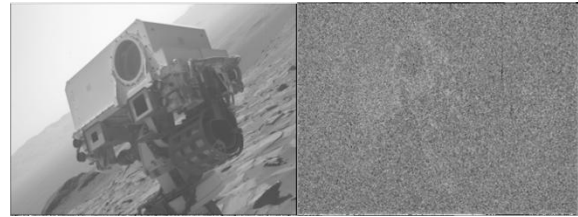
Figure 2: Pre-pointed daylight image (L) and average Phobos-shine image (R). Notice the faint signal acquired from Phobos-light reflecting off the RSM.

Observational Radiance calculation: The radiometric calibration pipeline outputs a radiance scaling factor to convert digital number values to units of I/F. As input flux is not directly relatable to DN value for MAHLI, A cross calibration method developed to obtain MAHLI radiance values through calibration with MastCam M34 was used [10].
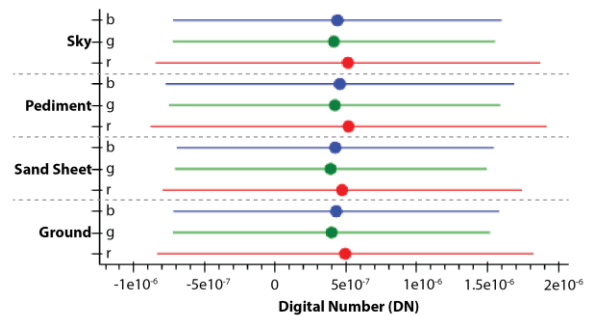
Figure 4: Mean digital number (DN) values for all pixels in each of the ROIs: sky, pediment, sand sheet, and foreground in the triboelectric observation indicating no significant difference between each area. Error bars 1σ.

Theoretical Radiance calculation: Theoretical radiance limits were also derived for comparison to the MAHLI triboelectric observational data. The following radiometric considerations that were used to produce these theoretical limits for the MAHLI G-band (500-600 nm; referred to a 'in-band'). Two quantities are estimated: (1) the solar radiance emitted directly by Phobos at the time of the "Phobos sky" observation, and (2) the radiance emitted by the RSM while illumi-

Empirical tribo-electric discharge	Theoretical upper limit	Observational upper limit
1.4-3.2 uW/m²/sr	0.23 uW/m²/sr	0.594 uW/m²/sr

nated only by Phobos-shine at the time of the "Phobos-shine" observation. The elevation of Phobos during the observation was 36 deg and azimuth of 278 deg.

Phobos-sky: The radiance [W/m²/sr], L_p, emitted by the surface of Phobos assuming Lambertian scattering is given by eq 1:

$$L_p = \frac{A_p}{\pi} \frac{F}{d^2} \quad (1)$$

where $F = 185$ W/m² is the in-band solar flux at 1AU, $d = 1.6$ AU is the Phobos-Sun distance at the time of the observation, and $A_p = 0.026$ is the albedo of the surface of Phobos at 550 nm [14]. To estimate the radiance that would be observed at the surface of Mars, L_p', the atmospheric attenuation must be accounted for using the Beer-Lambert law in eq 2:

$$L_p' = L_p e^{-\tau/\mu} \quad (2)$$

Where $\tau = 0.34$ is the atmospheric column opacity and is the cosine of the angle of incidence that accounts for the extended path length through the atmosphere. The Phobos-emitted radiance observed at the surface of Mars is therefore estimated as 0.28 W/m²/sr; normalized by the idealized Lambertian radiance (i.e. the solar radiance emitted by a normally illuminated ideal Lambertian surface) yields an I/F of 0.013.

Phobos-shine: the radiance reflected from the RSM can be estimated using the Phobos-emitted radiance L_p' calculated above. The flux incident on the RSM, F_{RSM}, due to Phobos-shine is given as $F_{RSM} = L_p'\Omega$, where Ω is the solid angle of Phobos' disk with respect to the Martian surface. The radiance reflected from the RSM toward the MAHLI imager can then be found using an assumption of Lambertian scattering and the albedo of the RSM, assumed here to be 0.9 [15] assuming a negligible change in reflectance due to dust settling. The incident flux on the RSM is calculated as 1.3 W/m² and the RSM-emitted radiance as 0.2 W/m²/sr.

It is noted the that observational and theoretical radiance values for Phobos-shine reflected off the RSM agree with each other, supporting the observationally derived upper limit for triboelectric discharge of ~0.6 uW/m²/sr.

Table 1: Empirical [3], and theoretical and observational radiance limits for triboelectric discharge at Gale Crater.

Establishing an upper threshold: There was no significant difference in the mean DN values between the four areas in the triboluminescence observation indicating that, if occurring, triboluminescence within the Sands of Forvie sand sheet was occurring below the radiance detection limit of MAHLI (figure 4). The absence of detection necessitated using the Phobos-shine observations to quantify an upper limit for putative triboelectric discharge assuming that Phobos-light reflected off of the RSM comprises the lowest signal capable of being detected by MAHLI. Using the MastCam cross-calibration pipeline, the radiance of reflected Phobos light is calculated as ~0.6 μW/m²/sr (table 1). Given the ionization energy of CH_4 of 12.61 eV, and assuming isotropic conditions, 100% ionization efficiency, and that CH_4 is well mixed in the lower 10-100 m of the atmosphere, then if occurring and producing a maximum radiance of ~0.6 μW/m²/sr, triboelectric discharge could ionize only 1 part in 1,000,000 to 1 part in 100,000 of the CH_4 emitted each night assuming a subsurface emission rate 5.6E15 CH_4 molecules/sol [16].

Implications for the near-surface atmosphere: Using ~0.6 μW/m²/sr as an upper limit for triboelectric discharge in a sand sheet near the end of the windy season at Gale crater, the number of molecules of CH_4 and O_2 that could be ionized are insufficient to have an appreciable effect on bulk methane or O_2 variability or explain the observed seasonal variation indicating that triboelectric discharge alone cannot account for the observed seasonal decrease in CH_4 and O_2 after ~Ls 150°. Several factors may explain the discrepancy between the empirical predictions and the observations. It is not currently known how often winds in Gale crater would reach the 21 m/s speed used in the empirical studies. Although there was some grain movement detected in the MARDI images, it was limited compared to the most active part of the windy season [6] and ripple migration was not observed suggesting low overall saltation fluxes. The time elapsed between the triboelectric observation and change detection observation precludes knowledge of the wind conditions during the main observation. Finally, the MastCam M34 cross-calibration pipeline relies on the I/F value calculated using the radiance scaling factor [17]. The radiance scaling factor assumes Solar illumination and may not be valid for night observations. To mitigate this challenge future work will model the predicted the radiance of reflected Phobos-light to quantify the signal captured by MAHLI during the

Phobos-shine observations providing an independent upper threshold on triboluminescence. Future observations of opportunity when sand sheets are in the MAHLI field of view at serval times during the windy season would place more robust limits on the potential occurrence of wind-mediated triboluminescence.

Conclusion: No evidence of saltation-mediated triboelectric discharge occurring above ~0.6 $\mu W/m^2/sr$ was detected within a sand sheet at Gale crater at the end of the windy season (L_s 356.3°) and triboluminescence is unlikely to be widespread enough, or producing a high enough flux to affect measurable concentrations of methane or oxygen in the near-surface atmosphere. The diurnal and seasonal variation of CH_4 remains enigmatic and a potential biosignature indicative of putative past of extant subsurface biological activity.

References:
1. Krauss, C.E., Horányi, M, M. & Robertson, S. *New J. Phys.* **5**, 70–70 (2003).
2. Krauss, C.E., Horányi, M, M. & Robertson, S *Journal of Geophysical Research* **11**, 8 (2006).
3. Thøgersen, J., Norskov Bak, E., Finster, K., Nørnberg, P. & Jakobsen, H.J. *Icarus* **332**, 14–18 (2019).
4. Greeley, R. et al. *J. Geophys. Res.* **111**, E02S09 (2006).
5. Geissler, P.E. et al. *Journal of Geophysical Research: Planets* **115**, (2010).
6. Baker, M.M. et al. *Geophys. Res. Lett.* **45**, 8853–8863 (2018).
7. Bridges, N.T. et al. *J. Geophys. Res.* **110**, E12004 (2005).
8. Conrad, R. *Environmental Microbiology Reports* **1**, 285–292 (2009).
9. Krasnopolsky, V.A., Maillard, J.P. & Owen, T. *Icarus* **172**, 537–547 (2004).
10. Harris, R.L. et al. *Sci Rep* **11**, 12336 (2021).
11. Trainer, M.G. et al. *Journal of Geophysical Research: Planets* **124**, 3000–3024 (2019).
12. Webster, C.R. et al. *Science* **360**, 1093–1096 (2018).
13. Edgett, K.S. et al. *Space Sci Rev* **170**, 259–317 (2012).
14. Pajola, M. et al. *ApJ* **777**, 127 (2013).
15. Wiens, R.C. et al. *Space Sci Rev* **170**, 167–227 (2012).
16. Moores, J.E. et al. *Nat. Geosci.* **12**, 321–325 (2019).
17. Liang, W. et al. *Icarus* **335**, 113361 (2020).